ity profile with much higher conductivity at lower potentials (Fig. 4) compared to PEDOT in the absence of air (fig. S5), indicating that the PEDOT is reaching a steady-state oxidation level according to the applied potential, which is greater in the presence of air. The mechanism of the air reduction electrocatalysis likely involves a redox cycling process where the PEDOT, which naturally rests in an oxidized form, is momentarily reduced by the action of the electrochemical cell. An O_2 molecule then absorbs onto the surface of the PEDOT and rapidly reoxidizes the PEDOT to its preferred oxidized state and is itself reduced in the process. The role of the counterion in this mechanism, if any, is still unclear.

Given the similarity between the Pt and PEDOT responses in Fig. 2, it seems likely that the O_2 reduction proceeds via the four-electron pathway as it does on Pt, because there is no sign of an additional process that might indicate a contribution from H_2O_2 formation. Further investigation of the type described by Halseid et al. (27) is under way to probe the selectivity with respect to the four-electron pathway. Recent reports (28) describe efficient iron-loaded graphite catalysts for oxygen reduction. Given the very low Fe loadings involved, we cannot exclude the possibility of a role for residual Fe, at levels below the limit of x-ray photoelectron spectroscopy detection, in the mechanism reported here. However, iron-based catalytic centers would normally be expected to show signs of poisoning in the presence of CO; the resistance to CO poisoning seen here (Fig. 3) thus suggests that iron centers do not play a notable role.

A laboratory Zn/air battery was also constructed based on this PEDOT air-electrode assembly and a 1 M KOH electrolyte. An open-circuit voltage of 1.44 V was measured, comparable with other examples of this cell (29, 30). Discharge characteristics (fig. S6) as a function of current density and over a 48-hour continuous test were superior to similar devices constructed with a Pt/Goretex air electrode.

The electrode described here provides only a partial solution to some of the problems with the use of Pt discussed in the introduction, because Pt is also used in the anode (fuel) electrode in the fuel cell. However, the fundamental mode of catalysis at work in the present materials may be able to be extended to other reactions, such as the hydrogen oxidation reaction, by careful choice of the ICP. ICPs can be successfully used as a substitute for Pt in dye-sensitized solar cells for the I^-/I_3^- redox reaction (31). Thus, the development of the gas-ICP-electrolyte three-phase interface electrode reported here may provide a platform for a new generation of metal-free electrocatalysts.

References and Notes

1. T. Teratani, R. Mizutani, K. Yamamoto, T. Anegawa, *IEEJ Trans. Electr. Electron. Eng.* **3**, 162 (2008).
2. P. Agnolucci, *Int. J. Hydrogen Energy* **32**, 3526 (2007).
3. E. Pucher, A. Sekanina, *Elektrotechnik und Informationstechnik* **123**, 410 (2006).
4. K. Jorgensen, *Utilities Policy* **16**, 72 (2008).
5. V. R. Stamenkovic et al., *Science* **315**, 493 (2007).
6. J. Zhang, K. Sasaki, E. Sutter, R. R. Adzic, *Science* **315**, 220 (2007).
7. University of Houston, "Fuel Cells Gearing Up To Power Auto Industry," *ScienceDaily*, 31 October 2007, retrieved 14 April 2008; www.sciencedaily.com/releases/2007/10/071030121117.htm.
8. X. Yu, S. Ye, *J. Power Sources* **172**, 145 (2007).
9. A. S. Arico, S. Srinivasan, V. Antonucci, *Fuel Cells* **1**, 133 (2001).
10. D. J. Ham, Y. K. Kim, S. H. Han, J. S. Lee, *Catal. Today* **132**, 117 (2008).
11. M. Winter, R. J. Brodd, *Chem. Rev.* **104**, 4245 (2004).
12. R. Liu et al., *J. Phys. Chem. B* **104**, 3518 (2000).
13. J. S. Lee, S. Locatelli, S. T. Oyama, M. Boudart, *J. Catal.* **125**, 157 (1990).
14. R. Bashyam, P. Zelenay, *Nature* **443**, 63 (2006).
15. A. Garsuch et al., *J. Electrochem. Soc.* **155**, B236 (2008).
16. R. C. M. Jakobs, L. J. J. Janssen, E. Barendrecht, *Electrochim. Acta* **30**, 1313 (1985).
17. N. F. Atta et al., *J. Chem. Soc. Chem. Commun.*, 1347 (1990).
18. M. Somasundrum, J. V. Bannister, *J. Chem. Soc. Chem. Commun.*, 1629 (1993).
19. M. C. Lefebvre, Z. Qi, P. G. Pickup, *J. Electrochem. Soc.* **146**, 2054 (1999).
20. G. Tourillon, F. Garnier, *J. Phys. Chem.* **88**, 5281 (1984).
21. B. Winther-Jensen, K. West, *Macromolecules* **37**, 4538 (2004).
22. D. M. de Leeuw, P. A. Kraakman, P. F. G. Bongaerts, C. M. J. Mutsaers, D. B. M. Klaassen, *Synth. Met.* **66**, 263 (1994).
23. B. Winther-Jensen et al., *Org. Electron.* **8**, 796 (2007).
24. B. Winther-Jensen et al., *Polymer* **49**, 481 (2008).
25. V. Khomenko, V. Barsulov, A. Katashinskii, *Electrochim. Acta* **50**, 1675 (2005).
26. D. Ivnitski, B. Branch, P. Atanassov, C. Apblett, *Electrochem. Commun.* **8**, 1204 (2006).
27. R. Halseid, M. Heinen, Z. Jusys, R. J. Behm, *J. Power Sources* **176**, 435 (2008).
28. E. Proietti, S. Ruggeri, J. P. Dodelet, *J. Electrochem. Soc.* **155**, B340 (2008).
29. A. A. Mohamad, *J. Power Sources* **159**, 752 (2006).
30. W. K. Chao, C. M. Lee, S. Y. Shieu, C. C. Chou, F. S. Shieu, *J. Power Sources* **177**, 637 (2008).
31. Y. Saito, W. Kubo, T. Kitamura, Y. Wada, S. Yanagida, *J. Photochem. Photobiol. Chem.* **164**, 153 (2004).
32. Funding of this work by the Australian Research Council (ARC) Centre of Excellence in Electromaterials Science is gratefully acknowledged, as is ARC Fellowship support for B.W.-J. (Australian Postdoctoral Fellowship) and D.R.M. (Federation Fellowship).

Structures of Neutral Au7, Au19, and Au20 Clusters in the Gas Phase

Philipp Gruene,[1] David M. Rayner,[2] Britta Redlich,[3] Alexander F. G. van der Meer,[3] Jonathan T. Lyon,[1] Gerard Meijer,[1] André Fielicke[1]*

The catalytic properties of gold nanoparticles are determined by their electronic and geometric structures. We revealed the geometries of several small neutral gold clusters in the gas phase by using vibrational spectroscopy between 47 and 220 wavenumbers. A two-dimensional structure for neutral Au7 and a pyramidal structure for neutral Au20 can be unambiguously assigned. The reduction of the symmetry when a corner atom is cut from the tetrahedral Au20 cluster is directly reflected in the vibrational spectrum of Au19.

Haruta et al.'s finding that dispersed gold nanoparticles show pronounced catalytic activity toward the oxidation of CO has triggered a gold rush in cluster chemistry (1). Although bulk gold is a classic example of chemical inertness (2), many later studies have confirmed the size-dependent reactivity of deposited gold clusters (3–6). Small particles of gold differ from the bulk because they contain edge atoms that have low coordination (7) and can adopt binding geometries that lead to a more reactive electronic structure (8). Thus, the secret of the catalytic properties of gold nanoparticles lies at least partly in their geometric structure. Structural information for deposited gold mono- and bilayers on titania has been obtained by using high-resolution electron energy–loss spectroscopy on CO adsorbates (9). Determining the three-dimensional (3D) structure of deposited gold nanoparticles is more challenging, but recently has been achieved for clusters containing around 310 atoms by means of aberration-corrected scanning transmission electron microscopy (10).

The geometry of nanoparticles can also be studied in the gas phase. The advantages of this approach are the exact knowledge of the clusters' size and the absence of any interaction with the surrounding environment. The properties of such well-defined species can thus be modeled very precisely with quantum-mechanical calculations. Different experimental techniques exist for the study of free clusters. By measuring the mobility of size-selected gold anions and cations in helium, a transition from 2D to 3D structures has been found (11, 12). This transition appears at different cluster sizes for cations and anions and is yet to be determined experimentally for neutral species. A combination of photoelectron spectroscopy and quantum-mechanical calculations has revealed fascinating structures of anionic gold species—for example, cages for clusters containing 16 to 18 atoms (13), a tetrahedral pyramid for Au_{20}^- (14), and a possibly chiral structure for Au_{34}^- (15). These structural motifs have been confirmed by measurement of the electron diffraction pattern of size-selected trapped anions (15, 16). Although ion mobility measurements, photoelectron spectrosco-

[1]Fritz-Haber-Institut der Max-Planck-Gesellschaft, 14195 Berlin, Germany. [2]Steacie Institute for Molecular Sciences, Ottawa, Ontario K1A 0R6, Canada. [3]Stichting voor Fundamenteel Onderzoek der Materie (FOM) Institute for Plasma Physics Rijnhuizen, 3439 MN Nieuwegein, Netherlands.

*To whom correspondence should be addressed. E-mail: fielicke@fhi-berlin.mpg.de

py, and trapped-ion electron diffraction have all substantially added to the understanding of the geometric properties of free nanoparticles, these methods are restricted to the investigation of charged species.

We investigated neutral gold clusters in the gas phase by means of vibrational spectroscopy, which is inherently sensitive to structure. In infrared (IR) absorption spectroscopy, the number of allowed transitions is restricted by selection rules, and thus directly reflects the symmetry of the particle. Far-IR multiple-photon dissociation (FIR-MPD) spectroscopy is a proven technique for obtaining the vibrational spectra of gas-phase metal clusters and, hence, by comparison with calculated spectra, their geometries (17, 18). It is the only technique for determining the structure of free metal clusters that is not

limited to charged species. We explored three representative sizes of neutral gold clusters. With Au_7, we investigated the structure in a size region in which the anions and cations are known to adopt planar structures, and we thereby addressed a controversy in theoretical studies. With Au_{20}, we confirmed that the neutral cluster retains the symmetrical pyramid geometry established for the anion. With Au_{19}, we directly observed the reduction of symmetry when one of the corner atoms is removed from Au_{20}.

Details of the technique of FIR-MPD have been described elsewhere (17, 19). Neutral gold clusters are produced by means of laser vaporization from a gold rod in a continuous flow of He and Kr (1.5% Kr in He) at 100 K. Under these conditions, complexes of the bare metal clusters with
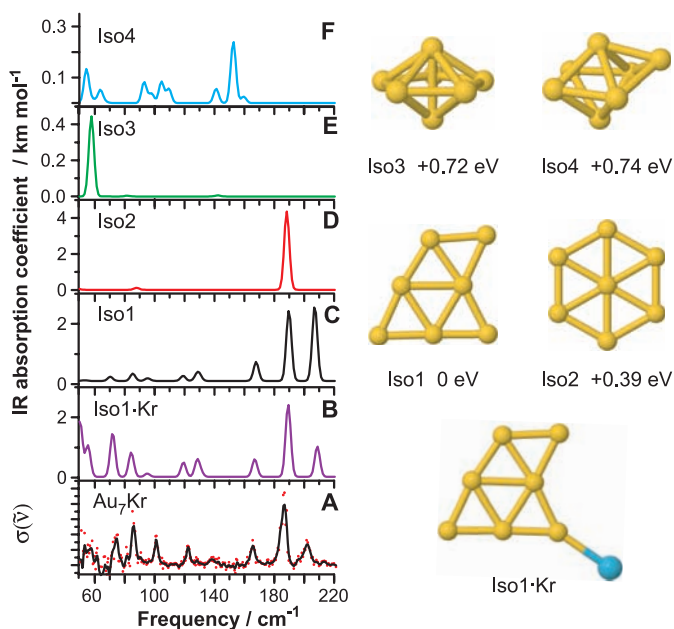
one or two Kr ligands are formed. The molecular beam is overlapped with a pulsed FIR beam delivered by the Free Electron Laser for Infrared eXperiments (FELIX) (20). The neutral complexes are ionized by an F_2-excimer laser (7.9 eV per photon) and mass-analyzed in a time-of-flight mass spectrometer. Resonance of the FIR light with an IR-active vibrational mode of a given neutral cluster may lead to the absorption of several photons. The subsequent heating of the complex results in the evaporation of a loosely bound Kr ligand and a depletion of the corresponding mass spectrometric signal. Recording the mass-spectrometric signal while scanning the wavelength of FELIX leads to depletion spectra, from which absorption spectra $\sigma(\tilde{\nu})$ are reconstructed (21).

Figure 1A shows the vibrational spectrum of neutral Au_7 obtained with FIR-MPD of its complex with one Kr ligand. A number of bands were found in the region between 47 and 220 cm^{-1}, usually having a full width at half maximum of less than 4 cm^{-1} (21). This is close to the spectral bandwidth of FELIX, which is about 2 to 3 cm^{-1} and nearly constant over the whole tuning range. The number of peaks implies a rather nonsymmetric structure for neutral Au_7. The geometry of Au_7 was established by comparing the experimental spectrum with the calculated vibrational spectra for multiple isomers predicted by density functional theory (DFT) calculations within the generalized gradient approximation (21, 22). We found a planar edge-capped triangle with C_s symmetry (Iso1) to be lowest in energy. This structure has been previously reported as the global minimum (23). A hexagonal planar structure (Iso2) (24) and a 3D structure (Iso3) (25) have been proposed as lowest-energy structures as well, but were computed to be higher in energy in the present study.

The experimental vibrational spectrum unambiguously tested the reliability of the theoretical methods. The calculated spectra were distinctive in the range between 150 and 220 cm^{-1}. The peak positions of Iso1 fit with experimental absorptions at 165, 186, and 201 cm^{-1}. Only the relative intensities of the bands did not agree completely; the central band at 186 cm^{-1} was much more pronounced in the experiment. Figure 1B shows the calculated absorption spectrum of the complex Iso1·Kr, in which Kr is bound to the energetically most favorable position of the Iso1 cluster with a bond dissociation energy of 0.09 eV. The positions of the resonances were not changed, but the relative intensities were substantially affected. The three bands were then in excellent agreement with the experiment, and, furthermore, all absorptions between 50 and 150 cm^{-1} became more pronounced (26). The calculations show that all of these vibrational modes are highly delocalized and involve the motion of all atoms in the cluster [see normal mode displacement vectors for the three highest-energy vibrations of Au_7 (all in-plane) in fig. S3].

In principle, multiple isomers can be present in the molecular beam, in which case the spectrum would represent a superposition of their individual contributions. Iso2 has one strong absorption at

Fig. 1. Vibrational spectra of neutral Au_7. (**A**) The FIR-MPD spectrum of Au_7Kr. The red dots represent relative cross sections, $\sigma(\tilde{\nu})$, the average of up to ~1000 single laser shots at a fixed frequency, whereas the black line interconnects a binomially weighted five-point running average, thus accounting for the spectral bandwidth of the IR laser. It is compared with the spectra of four low-lying isomers (Iso1 to 4) (**C** to **F**) obtained by DFT calculations. The peak positions in the experiment are in best agreement with a planar structure of C_s symmetry (Iso1). Including the Kr ligand in the calculation does not substantially change the structure of the cluster or the positions of the resonances (Iso1·Kr) (**B**), but has an effect on the IR intensities, which become very similar to those in the experimental spectrum.

Fig. 2. Vibrational spectra of neutral Au_{19} and Au_{20}. (**A** and **B**) The FIR-MPD spectra of Au_{20}Kr and Au_{19}Kr, respectively. (**C** and **D**) Calculated spectra for pyramidal geometries Au_{20} and Au_{19} are in excellent agreement with the experiment. The splitting of the degenerate resonance at 148 cm^{-1} for Au_{20} into two peaks at 149 cm^{-1} and 166 cm^{-1} for Au_{19} is due to the lowering of symmetry when going from the tetrahedron to the truncated pyramid.
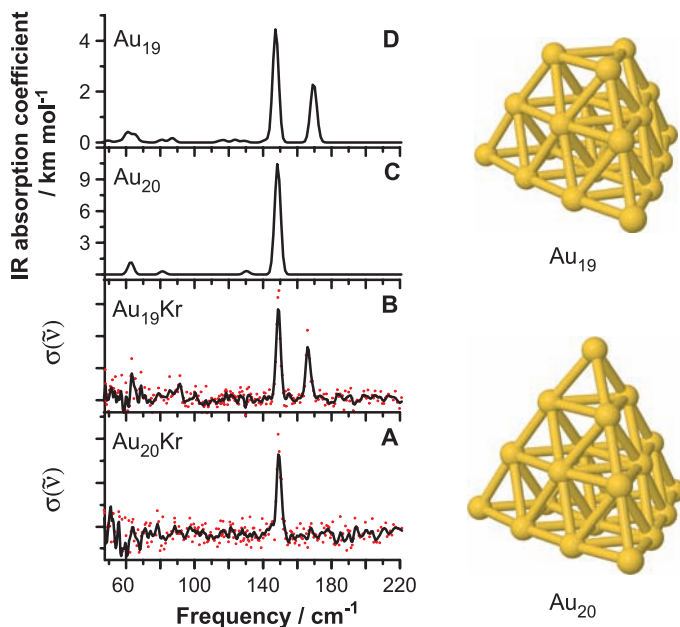
185 cm^{-1}, and its presence in the molecular beam could also explain the pronounced intensity of the central peak in the experimental spectrum. Ion mobility measurements, however, excluded the presence of major amounts of additional isomers for cationic and anionic Au$_7$. For experimental modes that were not present in the calculated spectrum of hexagonal Iso2—for example, at 165 cm^{-1} and 201 cm^{-1}—the mass-spectrometric intensity of Au$_7$Kr went down to below 30% of its original value when irradiated by FELIX, which set the upper limit for the abundance of other isomers. Therefore, although a minor contribution of Iso2 could not be ruled out, the capped triangle could be assigned as the dominant structural isomer of neutral Au$_7$ present in our experiment.

On comparison with the experimentally determined structures of the corresponding ionic species, we found that Au$_7$ is a cluster size, which changes its geometries for each charge state. Although the cation is highly symmetric and corresponds to the D_{6h} structure Iso2 (12), the anion forms a threefold edge-capped square (11). We found this structure to be a saddle point in our calculations for neutral Au$_7$ that relaxes into Iso1. The geometrical change as a function of cluster charge corresponds to a lessening of the average coordination as the electron density increases. Although the gold atoms in the cation have on average 3.43 nearest neighbors, this value decreases to 3.14 and 2.85 for the neutral and the anion, respectively. With additional electrons, the clusters favor more open structures.

Having shown that the experimental spectrum, in combination with theory, can be used to identify the geometry of the Au$_7$ cluster, we moved on to bigger sizes. Photoelectron spectroscopy and quantum-mechanical calculations have shown that anionic Au$_{20}^-$ is a pyramid and has T_d symmetry (14). This structure has also been suggested to be the global minimum for neutral Au$_{20}$ (14). The FIR-MPD spectrum we measured of the Au$_{20}$Kr complex (Fig. 2A) was very simple, with a dominant absorption at 148 cm^{-1}, which already pointed to a highly symmetric structure. The calculated spectrum of tetrahedral Au$_{20}$ was in agreement with the experiment (Fig. 2C, and see fig. S4 for the IR spectra of less stable isomers). In the FIR-MPD spectrum of Au$_{20}$Kr$_2$, weaker features occurred at low frequencies and were well reproduced by theory when the Kr ligands are included in the calculations (fig. S1). The strong absorption at 148 cm^{-1} corresponds to a triply degenerate vibration (t_2) in bare Au$_{20}$ with T_d symmetry.

Theory predicts a truncated trigonal pyramid to be the minimum energy structure for neutral Au$_{19}$ (27), for which the removal of a corner atom of the Au$_{20}$ tetrahedron reduces the symmetry from T_d to C_{3v}. As a direct consequence, the degeneracy of the t_2 vibration of Au$_{20}$ is lifted, and this mode splits into a doubly degenerate vibration (e) and a non-degenerate vibration (a_1) in Au$_{19}$. This splitting was observed in the vibrational spectrum of neutral Au$_{19}$ (Fig. 2). The e vibration lies at 149 cm^{-1} and is hardly shifted as compared with the t_2 mode of

Au$_{20}$. The a_1 vibration is blue-shifted by 18 cm^{-1} relative to the t_2 vibration in Au$_{20}$. The truncated pyramidal structure of Au$_{19}$ can thus be inferred directly from the IR spectrum. We also found the C_{3v} structure of Au$_{19}$ to be a minimum in our calculations, and the calculated vibrational spectrum fits the experimental one in terms of peak positions and relative intensities (Fig. 2D, and see fig. S5 for IR spectra of less-stable isomers). Again, the modifications in peak intensities induced by the Kr ligands agree well between theory and experiment (fig. S2).

We have shown that detailed structural information on small neutral gold nanoparticles can be obtained by means of vibrational spectroscopy. FIR-MPD is the only size-selective experimental technique available to date that allows for the structure determination of neutral metal clusters in the gas phase. It can be used to study the transition of 2D structures to 3D structures for neutral gold clusters as well as to study, for instance, ligand-induced geometrical modifications that are highly relevant in catalysis. With improved sensitivity for heavier masses, it will be possible to extend these measurements to larger clusters. Although spectral congestion may prohibit detailed analysis of non-symmetric structures, we can expect symmetric and near-symmetric structures to remain identifiable, as they do for Au$_{20}$ and Au$_{19}$. For instance, it should be possible to answer questions such as, is neutral Au$_{55}$ icosahedral, or does it have a low-symmetry structure such as has been indicated for the anion (28)?

References and Notes

1. M. Haruta, N. Yamada, T. Kobayashi, S. Iijima, J. Catal. **115**, 301 (1989).
2. B. Hammer, J. K. Nørskov, Nature **376**, 238 (1995).
3. M. Valden, X. Lai, D. W. Goodman, Science **281**, 1647 (1998).
4. B. Yoon et al., Science **307**, 403 (2005).
5. C. T. Campbell, Science **306**, 234 (2004).
6. P. P. Edwards, J. M. Thomas, Angew. Chem. Int. Ed. **46**, 5480 (2007).
7. C. Lemire, R. Meyer, S. Shaikhutdinov, H.-J. Freund, Angew. Chem. Int. Ed. **43**, 118 (2004).
8. G. Mills, M. S. Gordon, H. Metiu, J. Chem. Phys. **118**, 4198 (2003).
9. M. S. Chen, D. W. Goodman, Science **306**, 252 (2004).
10. Z. Y. Li et al., Nature **451**, 46 (2008).
11. F. Furche et al., J. Chem. Phys. **117**, 6982 (2002).
12. S. Gilb et al., J. Chem. Phys. **116**, 4094 (2002).
13. S. Bulusu, X. Li, L.-S. Wang, X. C. Zeng, Proc. Natl. Acad. Sci. U.S.A. **103**, 8326 (2006).
14. J. Li, X. Li, H.-J. Zhai, L.-S. Wang, Science **299**, 864 (2003).
15. A. Lechtken et al., Angew. Chem. Int. Ed. **46**, 2944 (2007).
16. X. Xing, B. Yoon, U. Landman, J. H. Parks, Phys. Rev. B **74**, 165423 (2006).
17. A. Fielicke et al., Phys. Rev. Lett. **93**, 023401 (2004).
18. A. Fielicke, C. Ratsch, G. von Helden, G. Meijer, J. Chem. Phys. **122**, 091105 (2005).
19. A. Fielicke, G. von Helden, G. Meijer, Eur. Phys. J. D **34**, 83 (2005).
20. D. Oepts, A. F. G. van der Meer, P. W. van Amersfoort, Infrared Phys. Technol. **36**, 297 (1995).
21. Materials and methods are available as supporting material on Science Online.
22. The IR frequencies, calculated by DFT with TURBOMOLE V5.10 (29), were uniformly scaled by multiplication with a factor of 1.15.
23. V. Bonačić-Koutecký et al, J. Chem. Phys. **117**, 3120 (2002).
24. H. Häkkinen, U. Landman, Phys. Rev. B **62**, R2287 (2000).
25. J. Wang, G. Wang, J. Zhao, Phys. Rev. B **66**, 035418 (2002).
26. The influence of the rare-gas ligand on the IR absorption intensities is very similar to what has been found in photodissociation studies of cationic gold clusters in the visible region (30).
27. S. Bulusu, X. C. Zeng, J. Chem. Phys. **125**, 154303 (2006).
28. W. Huang et al., ACS Nano **2**, 897 (2008).
29. R. Ahlrichs, M. Bär, M. Häser, H. Horn, C. Kölmel, Chem. Phys. Lett. **162**, 165 (1989).
30. A. N. Gloess, H. Schneider, J. M. Weber, M. M. Kappes, J. Chem. Phys. **128**, 114312 (2008).
31. The authors acknowledge support from the Cluster of Excellence Unifying Concepts in Catalysis coordinated by the Technische Universität Berlin and funded by the Deutsche Forschungsgemeinschaft. This work is supported by FOM by providing beam time for FELIX. We thank the FELIX staff for their skillful assistance, in particular J. Pluijgers and R. van Buuren, as well as K. Rademann for providing the cluster source. P.G. thanks the International Max Planck Research School Complex Surfaces in Material Science, and J.T.L. thanks the Alexander von Humboldt Foundation for funding.

Colossal Ionic Conductivity at Interfaces of Epitaxial ZrO$_2$:Y$_2$O$_3$/SrTiO$_3$ Heterostructures

J. Garcia-Barriocanal,[1] A. Rivera-Calzada,[1] M. Varela,[2] Z. Sefrioui,[1] E. Iborra,[3] C. Leon,[1] S. J. Pennycook,[2] J. Santamaria[1]*

The search for electrolyte materials with high oxygen conductivities is a key step toward reducing the operation temperature of fuel cells, which is currently above 700°C. We report a high lateral ionic conductivity, showing up to eight orders of magnitude enhancement near room temperature, in yttria-stabilized zirconia (YSZ)/strontium titanate epitaxial heterostructures. The enhancement of the conductivity is observed, along with a YSZ layer thickness–independent conductance, showing that it is an interface process. We propose that the atomic reconstruction at the interface between highly dissimilar structures (such as fluorite and perovskite) provides both a large number of carriers and a high-mobility plane, yielding colossal values of the ionic conductivity.

Solid oxide fuel cells (SOFCs) have emerged as a promising nonpolluting technology for the short-to-medium–term substitution

of fossil fuels (1–4). The conversion efficiency of chemical into electrical energy is limited by the transport of oxygen anions through an elec-

Science

Structures of Neutral Au$_7$, Au$_{19}$, and Au$_{20}$ Clusters in the Gas Phase

Philipp Gruene, David M. Rayner, Britta Redlich, Alexander F. G. van der Meer, Jonathan T. Lyon, Gerard Meijer and André Fielicke

ARTICLE TOOLS	http://science.sciencemag.org/content/321/5889/674
SUPPLEMENTARY MATERIALS	http://science.sciencemag.org/content/suppl/2008/07/31/321.5889.674.DC1
REFERENCES	This article cites 27 articles, 6 of which you can access for free http://science.sciencemag.org/content/321/5889/674#BIBL
PERMISSIONS	http://www.sciencemag.org/help/reprints-and-permissions

Use of this article is subject to the Terms of Service